

Article

Online Learning for Reference-Based Super-Resolution

Byungjoo Chae ^{1,†}, Jinsun Park ^{2,†} , Tae-Hyun Kim ³ and Donghyeon Cho ^{1,*} 

¹ Department of Electronics Engineering, Chungnam National University, 99 Daehak-ro, Yuseong-gu, Daejeon 34134, Korea; wpdhkd1642@gmail.com

² School of Computer Science and Engineering, Pusan National University, 2 Busandaehak-ro 63beon-gil, Geumjeong-gu, Busan 46241, Korea; jspark@pusan.ac.kr

³ Department of Computer Science, Hanyang University, 222 Wangsimni-ro, Seongdong-gu, Seoul 04763, Korea; taehyunkim@hanyang.ac.kr

* Correspondence: cdh12242@cnu.ac.kr; Tel.: +82-42-821-5667

† These authors contributed equally to this work.

Abstract: Online learning is a method for exploiting input data to update deep networks in the test stage to derive potential performance improvement. Existing online learning methods for single-image super-resolution (SISR) utilize an input low-resolution (LR) image for the online adaptation of deep networks. Unlike SISR approaches, reference-based super-resolution (RefSR) algorithms benefit from an additional high-resolution (HR) reference image containing plenty of useful features for enhancing the input LR image. Therefore, we introduce a new online learning algorithm, using several reference images, which is applicable to not only RefSR but also SISR networks. Experimental results show that our online learning method is seamlessly applicable to many existing RefSR and SISR models, and that improves performance. We further present the robustness of our method to non-bicubic degradation kernels with in-depth analyses.

Keywords: reference-based SR; online learning; self-supervised learning



Citation: Chae, B.; Park, J.; Kim, T.-H.; Cho, D. Online Learning for Reference-Based Super-Resolution. *Electronics* **2022**, *11*, 1064. <https://doi.org/10.3390/electronics11071064>

Academic Editor: Savvas A. Chatzichristofis

Received: 28 February 2022

Accepted: 24 March 2022

Published: 28 March 2022

Publisher's Note: MDPI stays neutral with regard to jurisdictional claims in published maps and institutional affiliations.



Copyright: © 2022 by the authors. Licensee MDPI, Basel, Switzerland. This article is an open access article distributed under the terms and conditions of the Creative Commons Attribution (CC BY) license (<https://creativecommons.org/licenses/by/4.0/>).

1. Introduction

Deep learning-based single-image super-resolution (SISR) algorithms [1–9] have shown remarkable progress in recent years. However, these algorithms still suffer from blurry output images because they are generally trained to minimize the mean squared error (MSE) or mean absolute error (MAE) between the network output and ground truth images. This problem has led to various efforts to generate high-frequency details with a generative adversarial network (GAN) and/or perceptual losses [10–12]. However, these methods often lead to reduced reconstruction performance with unexpected visual artifacts. The reason for this is that GAN-based deep networks often generate visually pleasing images, but fail to recover genuine information lost during the downsampling (degradation) process. In order to reconstruct the lost information, reference-based super-resolution (RefSR) methods have been proposed. RefSR algorithms aim to benefit from rich high-frequency details of an external high-quality reference image such as video frames [13,14] or similar web images [15] during the reconstruction, and many RefSR methods attempt to align and combine information from a low-resolution (LR) input image and a high-resolution (HR) reference image to synthesize a HR image. To this end, most of the studies so far have explored how to find similar features and match the features [16–18] of the LR image and the reference image well. For instance, patch matching [19], deformable convolution [20], and attention [21] techniques have been utilized. The aforementioned methods have succeeded in transferring the high-frequency detail of a reference image. However, these reference-based algorithms show performance degradation when irrelevant high-resolution images are given as references. To this end, we present an online learning technique inspired by zero-shot super-resolution (ZSSR) [22]. In ZSSR, a LR input image

I^{LR} and its downsampled version $I^{LR} \downarrow$ are used for supervision during the inference phase. However, ZSSR has difficulties when dealing with a large scaling factor (e.g., $\times 3$, $\times 4$).

Therefore, in this paper, we propose a method to effectively exploit both LR and HR reference images for online learning to update not only RefSR but also SISR models. Furthermore, using a pre-trained SR model, we create a pseudo-HR image from a LR input image, then use this pair of a pseudo-HR images \bar{I}^{HR} and a downsampled pseudo-HR image $\bar{I}^{HR} \downarrow$ as another datum for the online learning of the SR model. In summary, we perform online learning for both SISR and RefSR models by utilizing three types of supervision, including I^{LR} , I^{Ref} , and \bar{I}^{HR} . We use not only each supervision individually, but also combinations of each supervision for online learning. As a result, the proposed method can benefit from more images during the online adaptation, compared with ZSSR [22].

Our key contributions can be summarized as follows:

- We propose an online learning method for reference-based super-resolution with various data pairs for supervision. To this end, we present three methods for SISR models and four methods for RefSR models;
- Our method is very simple, but it is effective, and can be seamlessly combined with both SISR and RefSR models;
- Our method shows consistent performance improvements without being significantly affected by the degree of similarity between the reference and input images.

2. Related Works

In this section, we review deep learning-based SISR and RefSR methods. Then, we introduce recent SR approaches using online adaptation.

Single-image super-resolution (SISR) restores high-frequency details of a LR image using only an input LR image. The traditional SISR approaches [23,24] usually exploit the self-similarity or self-recurrence of the input LR image. With deep learning, Dong et al. [25] introduced a SISR model with just three convolutional layers and outperformed traditional SISR methods with large margins. Kim et al. [3,4] increased the SR performance in terms of PSNR and SSIM by using very deep convolutional layers. Lai et al. [26] suggested LapSRN, which progressively restores high-frequency details with the Laplacian pyramid. Lim et al. [5] does away with unnecessary modules in residual networks such as batch normalization layers, and achieved improved performance. Zhang et al. [7] introduced a channel attention model to take care of the inter-dependency across different channels. The aforementioned methods have significantly increased SR performance in terms of PSNR and SSIM. However, these methods may be blurry or visually unpleasing to human eyes. To enhance visual quality, Johnson et al. [12] proposed perceptual loss that minimizes errors on high-level features. Ledig et al. [11] adopted the GAN framework to generate photo-realistic images. Furthermore, Wang et al. [27] introduced a relativistic adversarial loss based on a residual-in-residual dense block to produce more realistic images. Perception-based methods have succeeded in producing visually good results, but there is a limit to recovering information lost during the downsampling process.

Unlike SISR, reference-based image super-resolution (RefSR) uses an additional HR reference image as an input to restore high-frequency details. Therefore, information lost in the downsampling process can be obtained from the reference image. Zheng et al. [19] proposed RefSR-Net to combine information of both LR and reference images based on patch matching. Specifically, RefSR-Net extracts local patches from both LR and reference images and then searches for correspondences between them. After that, the resulting matches are used to synthesize a HR image. However, the patch-match-based approach has difficulty with handling non-rigid deformations and, thus, suffers from blur or grid artifacts. Using optical flow [28,29] for pixel-wise matching, Zheng et al. [30] presented CrossNet, combining a warping process and image synthesis. CrossNet can effectively handle non-rigid deformations between the input and reference images; however, it is vulnerable to large displacements. With the recent progress of neural-style transfer [31,32], Zhang et al. [33] proposed SRNTT, performing texture transfer from the reference image.

This is particularly robust when an unrelated reference image is paired with an input image. Shim et al. [20] proposed SSEN, which aligns features of input and reference images using non-local blocks and deformable convolutions. Intra-image global similarities extracted from non-local blocks are utilized to estimate relative offset to relevant reference features. After that, deformable convolution operations are used to align reference features to those from the input low-resolution image. It is an end-to-end trainable network that does not require optical flow estimation or explicit patch-match. Yang et al. [21] introduced an attention-based RefSR method called TTSR, and have achieved significant performance improvements. Recently, Jiang et al. [34] presented a knowledge-distillation technique to solve the matching difficulties caused by the scale difference between the reference image and the LR input image. Lu et al. [35] introduced the MASA network for addressing the computational burden problem that may occur in LR image and reference image matching. However, these methods are sensitive to the similarity of the reference image.

Recently, Shocher et al. [22] proposed a zero-shot super-resolution that makes the CNN model flexibly adapt to the test image. In other words, parameters of the CNN model are updated during the test phase, and a CNN model optimized for the input image can be obtained. Furthermore, to reduce the number of updates, meta-learning techniques are applied in [36,37]. In this paper, as the first study to apply online learning to the RefSR problem, we achieved robust RefSR despite the difference in similarity between input and reference images.

3. Methods

In this section, we introduce our online learning methods for the RefSR problem using both SISR and RefSR models. We then describe the inference process of our method.

3.1. Online Learning

In online learning, the most important point is how to exploit input data given at the test phase. Online learning exploits self-similarity in the image. Using the characteristics of online learning to learn internal features, we proceed with high-resolution reference images with similar characteristics and use them to recover test images to improve performance.

For the RefSR problem, this is more crucial, because two kinds of input data are available: a LR image I^{LR} and the reference image I^{Ref} . Therefore, we develop various methods to construct pairs of train-input X and train-target (supervision) Y from multiple images (i.e., I^{LR} , I^{Ref}). Although our main goal is to solve the RefSR problem in this work, we present methods to construct pairs of data D which can be used to train not only RefSR but also SISR models at the test time.

3.1.1. SISR Model

Existing SISR models require data pairs D_s consisting of an input X and supervision Y (i.e., $D_s = \{X, Y\}$) for training. To be specific, we present three strategies, D_s^{LR} , D_s^{Pse} , and D_s^{Ref} , to construct D_s . First, D_s^{LR} consists of a downsampled LR image and an input LR image and is denoted by $D_s^{LR} = \{X : I^{LR} \downarrow, Y : I^{LR}\}$. Note that this is a commonly used configuration to exploit self-similarity in SISR such as ZSSR [22]. Next, D_s^{Pse} is constructed with a pseudo-HR image \bar{I}^{HR} obtained from a pre-trained SR model $\mathbf{P}_\phi(\cdot)$ as follows:

$$\bar{I}^{HR} = \mathbf{P}_\phi(I^{LR}), \quad (1)$$

where ϕ is the pre-trained network parameter. Then, we downsample \bar{I}^{HR} to construct a pair of training samples, and the set is defined as $D_s^{Pse} = \{X : \bar{I}^{HR} \downarrow, Y : \bar{I}^{HR}\}$. Finally, we utilize a reference image for D_s^{Ref} . Similar to D_s^{LR} and D_s^{Pse} , a downsampled image and the original reference images are paired as $D_s^{Ref} = \{X : I^{Ref} \downarrow, Y : I^{Ref}\}$. Using these three

data pairs acquired in the test phase, pre-trained parameters θ_s of a SISR model $\mathbf{SISR}_{\theta_s}(\cdot)$ are updated by minimizing the following loss function:

$$\mathcal{L}_{\theta_s}(x, y) = \mathbf{E}[||\mathbf{SISR}_{\theta_s}(x) - y||], \quad (2)$$

where x and y are extracted patches from X and Y in D_s . Note that the aforementioned data pairs can be used individually or in combination.

3.1.2. RefSR Model

In order to train RefSR models, a pair of data D_r that comprises an input X , a reference R , and supervision Y (i.e., $D_r = \{X, R, Y\}$) is required. Thanks to the additional input R , it is possible to construct more diverse data pairs than SISR models, and we propose four methods to construct D_r : D_r^{LR} , D_r^{Pse} , D_r^{Ref1} , and D_r^{Ref2} . First, D_r^{LR} is composed of a downsampled LR image, a reference image, and an input LR image, and denoted by $D_r^{LR} = \{X : I^{LR} \downarrow, R : I^{Ref}, Y : I^{LR}\}$ (cf., D_s^{LR}). Similarly, we define the second data pair $D_r^{Pse} = \{X : \bar{I}^{HR} \downarrow, R : I^{Ref}, Y : \bar{I}^{HR}\}$ by including I^{Ref} to D_s^{Pse} as a reference R . In addition, we can utilize a downsampled reference image $I^{Ref} \downarrow$ and the original one I^{Ref} as an input X and supervision Y , respectively, and an input LR image as a reference R to make the third data pair $D_r^{Ref1} = \{X : I^{Ref} \downarrow, R : I^{LR}, Y : I^{Ref}\}$. Finally, we replace I^{LR} in D_r^{Ref1} with \bar{I}^{HR} to make the last data pair $D_r^{Ref2} = \{X : I^{Ref} \downarrow, R : \bar{I}^{HR}, Y : I^{Ref}\}$. Note that D_r^{Ref1} and D_r^{Ref2} are extended from D_s^{Ref} by adding I^{LR} and \bar{I}^{HR} as the reference. With these data pairs, we can update network parameters θ_r of the pre-trained RefSR model $\mathbf{RefSR}_{\theta_r}(\cdot)$ with the following loss function:

$$\mathcal{L}_{\theta_r}(x, r, y) = \mathbf{E}[||\mathbf{RefSR}_{\theta_r}(x, r) - y||], \quad (3)$$

where x , r and y are extracted patches from X , R , and Y in D_r . Similar to SISR models, data pairs can be used individually or combined for online learning. The data pairs for online learning of SISR and RefSR models are summarized in Table 1.

Table 1. Online learning data pairs for SISR and RefSR models.

Model	SISR			RefSR			
Data Pair	D_s^{LR}	D_s^{Pse}	D_s^{Ref}	D_r^{LR}	D_r^{Pse}	D_r^{Ref1}	D_r^{Ref2}
X	$I^{LR} \downarrow$	$\bar{I}^{HR} \downarrow$	$I^{Ref} \downarrow$	$I^{LR} \downarrow$	$\bar{I}^{HR} \downarrow$	$I^{Ref} \downarrow$	$I^{Ref} \downarrow$
R	-	-	-	I^{Ref}	I^{Ref}	I^{LR}	\bar{I}^{HR}
Y	I^{LR}	\bar{I}^{HR}	I^{Ref}	I^{LR}	\bar{I}^{HR}	I^{Ref}	I^{Ref}

3.2. Inference

With the updated parameters of SISR or RefSR models at the test stage, we estimate the final super-resolved output image as follows:

$$\bar{O}_s = \mathbf{SISR}_{\theta_s}(I^{LR}), \quad \bar{O}_r = \mathbf{RefSR}_{\theta_r}(I^{LR}, I^{Ref}). \quad (4)$$

Notably, unlike RefSR, SISR models are updated using the reference image in the online learning phase, but the reference image is not used for the final inference.

4. Experiments

In this section, we describe implementation details and demonstrate both quantitative and qualitative comparisons with existing methods. We also provide various empirical analyses, including experiments according to the similarity between the reference image and the input LR image and experiments using non-bicubic degradation LR images.

4.1. Implementation Details

For both SISR and RefSR models, we used the CUFED dataset [33], which consists of 11,871 pairs of input and reference images to pre-train the models for $\times 4$ upscaling. As baseline SISR models, we have adopted light-weight versions of SimpleNet [22], RCAN [7], and EDSR [5] for fast execution time. Specifically, the number of residual blocks is reduced from 20 to 6 for the RCAN, and from 32 to 16 for EDSR with 64 feature dimensions. Each model is trained for 100 epochs with 32 batch sizes. We use all training data, including both HR and reference images. For RefSR models, SSEN [20] and TTSR [21] are adopted. SSEN is trained for 200 epochs with a batch size of 32, and TTSR is trained for 200 epochs with a batch size of 9. In the online learning phase, the CUFED5 dataset [33] is used. It consists of 126 groups of images, and each group contains a HR image and 5 reference images with different levels of similarity. Images are augmented with random crop (128×128), rotation, and flip. The initial learning rate is set to 1×10^{-4} for ADAM, and we multiply by 0.1 when the loss values stop decreasing [22]. Our method is implemented using PyTorch on Ubuntu 16.04 with a single RTX 2080 GPU.

4.2. Experimental Results

For all experiments, we have trained SISR and RefSR models by following their original configurations to obtain the baseline models. After that, the proposed online learning is applied to verify the effectiveness of our algorithm. Note that our method does not introduce any additional modules to the baseline models. All the models are evaluated on the CUFED5 test set. We evaluate in terms of PSNR, SSIM, and LPIPS [12], and the LPIPS value is measured with the VGG model.

Table 2 shows SISR online learning results over the baseline models. Online learning with only D_s^{LR} degrades performance in all models because the size of D_s^{LR} is too small (30×20) to exploit abundant information. In contrast, D_s^{Pse} contains plenty of HR details useful for the inference and, thus, performance is consistently improved with D_s^{Pse} as in [38]. Notably, we see further improvement by combining D_s^{LR} with D_s^{Pse} . Different from the results using D_s^{LR} only, $D_s^{LR} + D_s^{Pse}$ can effectively benefit from D_s^{LR} for self-similarity while keeping knowledge of HR information from D_s^{Pse} .

Table 2. SISR online learning results on SISR models.

Model	Method	PSNR	SSIM	LPIPS
SRCNN [9]	Pre-trained	25.475	0.737	0.3369
	D_s^{LR}	25.379	0.732	0.3388
	D_s^{Pse}	25.563	0.741	0.3273
	$D_s^{LR} + D_s^{Pse}$	25.559	0.741	0.3275
VDSR [3]	Pre-trained	25.660	0.746	0.3332
	D_s^{LR}	25.500	0.740	0.3229
	D_s^{Pse}	25.709	0.748	0.3256
	$D_s^{LR} + D_s^{Pse}$	25.734	0.749	0.3245
SimpleNet [22]	Pre-trained	25.800	0.753	0.3267
	D_s^{LR}	25.727	0.750	0.3128
	D_s^{Pse}	25.941	0.757	0.3152
	$D_s^{LR} + D_s^{Pse}$	25.958	0.757	0.3136
EDSR [5]	Pre-trained	26.198	0.771	0.2955
	D_s^{LR}	26.132	0.765	0.2897
	D_s^{Pse}	26.422	0.774	0.2956
	$D_s^{LR} + D_s^{Pse}$	26.440	0.775	0.2932
RCAN [7]	Pre-trained	26.243	0.774	0.2906
	D_s^{LR}	26.147	0.767	0.2883
	D_s^{Pse}	26.500	0.777	0.2912
	$D_s^{LR} + D_s^{Pse}$	26.512	0.778	0.2892

RefSR online learning results on the SISR baseline models are shown in Table 3. In RefSR online learning, baseline models always show performance improvements with D_s^{Ref} because it contains real high-frequency details not available in D_s^{Pse} . We achieve the best results by using both D_s^{LR} and D_s^{Ref} , rather than using either D_s^{LR} or D_s^{Ref} , respectively. Similar results are observed with RefSR online learning on the RefSR models where the best performance is mostly achieved with $D_r^{Pse} + D_r^{Ref2}$, as shown in Table 4. Figure 1 shows qualitative comparisons between existing methods and ours. Note that Figure 1f,k show superior performance over their baseline counterparts Figure 1e,j.

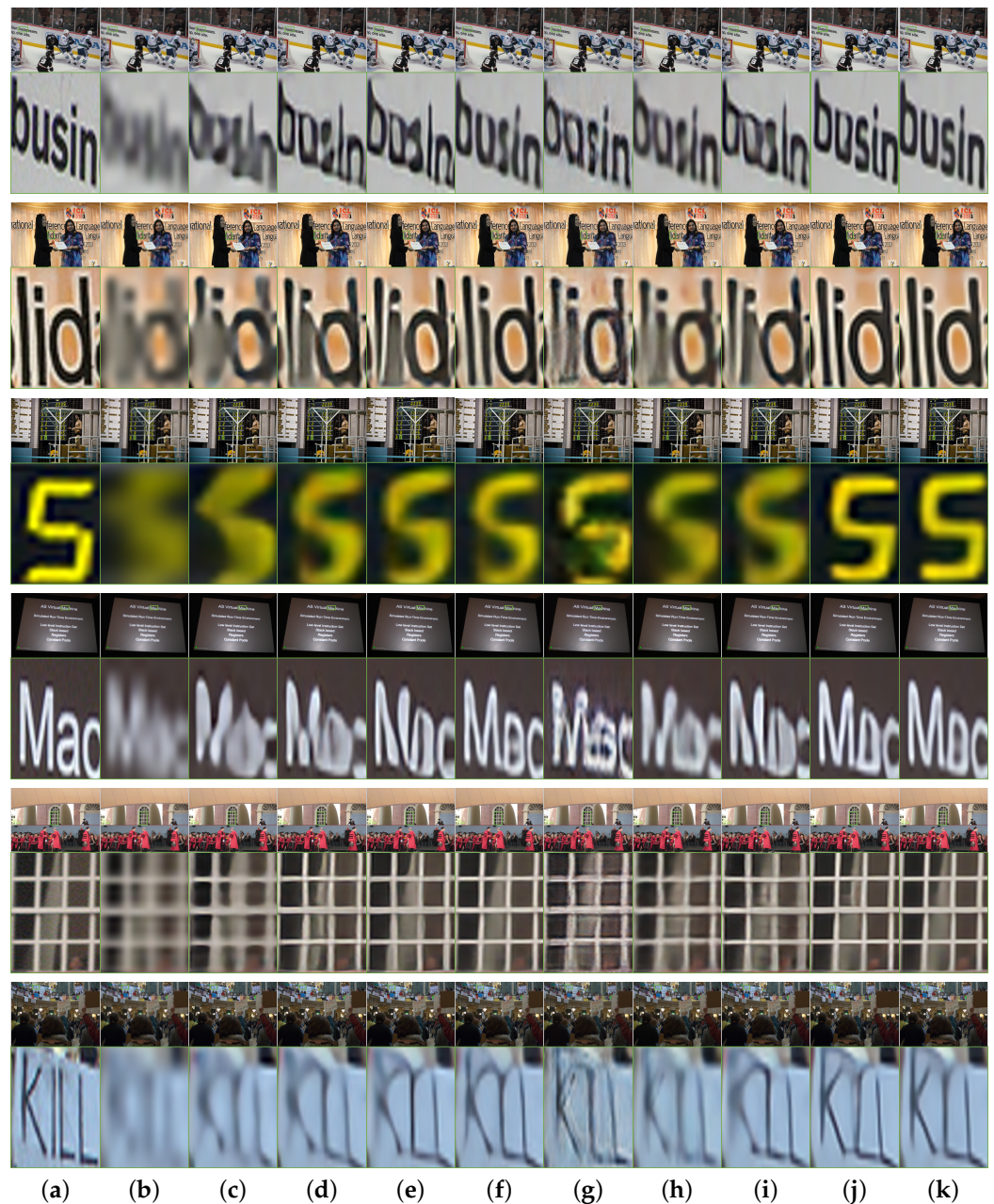


Figure 1. Qualitative comparison of RefSR methods on the CUFED5 datasets. (a) GT images. (b–k) Results of Bicubic, SimpleNet [22], EDSR [5], RCAN [7], Ours+RCAN [7], SRNTT [33], SRNTT- ℓ_2 [33], SSEN [20], TTSR-rec [21], and Ours+TTSR-rec [21], respectively.

Table 3. RefSR online learning results on SISR models.

Model	Method	Similarity														
		XL			L			M			H			XH		
		PSNR	SSIM	LPIPS	PSNR	SSIM	LPIPS	PSNR	SSIM	LPIPS	PSNR	SSIM	LPIPS	PSNR	SSIM	LPIPS
Ours + SimpleNet [22]	D_s^{Ref}	25.888	0.755	0.3159	25.932	0.756	0.3153	25.925	0.757	0.3148	25.990	0.758	0.3140	26.046	0.760	0.3127
	$D_s^{LR} + D_s^{Ref}$	25.894	0.755	0.3134	25.960	0.757	0.3119	25.950	0.758	0.3115	26.003	0.758	0.3107	26.058	0.761	0.3093
	$D_s^{Pse} + D_s^{Ref}$	25.936	0.757	0.3147	25.963	0.758	0.3145	25.979	0.758	0.3143	25.985	0.758	0.3140	26.018	0.759	0.3134
	$D_s^{LR} + D_s^{Pse} + D_s^{Ref}$	25.973	0.758	0.3131	25.991	0.758	0.3130	25.997	0.759	0.3130	26.010	0.759	0.3129	26.049	0.760	0.3122
Ours + EDSR [5]	D_s^{Ref}	26.354	0.772	0.2959	26.418	0.773	0.2937	26.417	0.774	0.2932	26.512	0.776	0.2922	26.645	0.780	0.2888
	$D_s^{LR} + D_s^{Ref}$	26.385	0.773	0.2889	26.438	0.775	0.2875	26.444	0.775	0.2875	26.553	0.777	0.2861	26.699	0.782	0.2833
	$D_s^{Pse} + D_s^{Ref}$	26.452	0.775	0.2949	26.467	0.775	0.2944	26.500	0.776	0.2935	26.497	0.776	0.2938	26.559	0.778	0.2926
	$D_s^{LR} + D_s^{Pse} + D_s^{Ref}$	26.462	0.775	0.2925	26.484	0.776	0.2922	26.508	0.776	0.2916	26.522	0.776	0.2917	26.577	0.778	0.2902
Ours + RCAN [7]	D_s^{Ref}	26.402	0.773	0.2919	26.465	0.775	0.2906	26.465	0.775	0.2900	26.581	0.778	0.2886	26.703	0.782	0.2856
	$D_s^{LR} + D_s^{Ref}$	26.418	0.774	0.2862	26.499	0.777	0.2853	26.505	0.777	0.2845	26.635	0.780	0.2828	26.810	0.785	0.2796
	$D_s^{Pse} + D_s^{Ref}$	26.511	0.777	0.2908	26.547	0.778	0.2901	26.567	0.778	0.2901	26.589	0.779	0.2895	26.634	0.781	0.2887
	$D_s^{LR} + D_s^{Pse} + D_s^{Ref}$	26.543	0.778	0.2890	26.562	0.779	0.2885	26.574	0.779	0.2884	26.607	0.780	0.2877	26.681	0.782	0.2862

Table 4. RefSR online learning results on RefSR models.

Model	Method	Similarity														
		XL			L			M			H			XH		
		PSNR	SSIM	LPIPS	PSNR	SSIM	LPIPS	PSNR	SSIM	LPIPS	PSNR	SSIM	LPIPS	PSNR	SSIM	LPIPS
SRNTT [33]	Pre-trained	25.14	0.729	0.2476	25.07	0.720	0.2410	25.06	0.728	0.2354	25.13	0.734	0.2294	25.17	0.734	0.2099
SRNTT- ℓ_2 [33]	Pre-trained	25.87	0.757	0.2949	25.88	0.758	0.2916	25.90	0.758	0.2893	25.97	0.760	0.2856	26.06	0.765	0.2758
SSEN [20]	Pre-trained	26.156	0.768	0.2979	26.151	0.768	0.2980	26.149	0.768	0.2979	26.154	0.768	0.2977	26.152	0.769	0.2976
Ours + SSEN [20]	D_r^{LR}	26.109	0.764	0.2879	26.107	0.764	0.2881	26.116	0.764	0.2889	26.108	0.764	0.2883	26.112	0.764	0.2884
	D_r^{Pse}	26.434	0.774	0.2951	26.459	0.775	0.2946	26.480	0.775	0.2944	26.480	0.775	0.2940	26.527	0.777	0.2930
	D_r^{Ref1}	26.226	0.767	0.2931	26.206	0.768	0.2925	26.241	0.768	0.2921	26.284	0.769	0.2903	26.276	0.770	0.2895
	D_r^{Ref2}	26.343	0.771	0.2946	26.383	0.772	0.2936	26.475	0.774	0.2920	26.509	0.775	0.2911	26.675	0.780	0.2874
	$D_r^{LR} + D_r^{Ref1}$	26.205	0.767	0.2852	26.206	0.767	0.2856	26.221	0.767	0.2854	26.261	0.768	0.2843	26.257	0.769	0.2946
	$D_r^{Pse} + D_r^{Ref2}$	26.392	0.773	0.2955	26.460	0.774	0.2942	26.475	0.774	0.2946	26.505	0.775	0.2935	26.568	0.777	0.2924
TTSR-rec [21]	Pre-trained	26.586	0.783	0.2825	26.623	0.785	0.2800	26.685	0.787	0.2782	26.787	0.789	0.2759	27.039	0.799	0.2653
Ours + TTSR-rec [21]	D_r^{LR}	26.407	0.775	0.2711	26.455	0.776	0.2689	26.502	0.778	0.2675	26.579	0.780	0.2643	26.812	0.788	0.2545
	D_r^{Pse}	26.822	0.786	0.2815	26.866	0.788	0.2792	26.937	0.790	0.2782	27.027	0.791	0.2760	27.337	0.801	0.2663
	D_r^{Ref1}	26.540	0.778	0.2791	26.563	0.781	0.2757	26.622	0.782	0.2750	26.769	0.785	0.2712	26.986	0.794	0.2614
	D_r^{Ref2}	26.658	0.782	0.2818	26.717	0.785	0.2788	26.836	0.787	0.2757	26.959	0.790	0.2730	27.383	0.802	0.2578
	$D_r^{LR} + D_r^{Ref1}$	26.497	0.777	0.2696	26.522	0.779	0.2668	26.592	0.780	0.2660	26.698	0.782	0.2635	26.900	0.790	0.2529
	$D_r^{Pse} + D_r^{Ref2}$	26.845	0.786	0.2816	26.877	0.788	0.2796	26.980	0.790	0.2780	27.056	0.792	0.2760	27.400	0.801	0.2663

4.3. Empirical Analyses

- **Reference Similarity**

We first analyze the effect of similarity of reference images on online learning. The CUFED5 dataset [33] provides five similarity levels, from the lowest (i.e., XL) to the highest (i.e., XH), depending on the content similarity between the reference and LR images. For both SISR and RefSR models, performance improvement is proportional to the level of similarity, and the best performance is obtained with the reference with the highest similarity XH. This result is expected, because XH reference images contain a large amount of real high-frequency details closely related to the lost details of LR images. Therefore, online learning with XH reference images can train baseline models with strong and relevant HR guidance. On the contrary, the amount of relevant information is reduced with decreasing similarity of the reference images; therefore, performance improvement also decreases, as shown in Tables 3 and 4.

- **Pseudo HR vs. LR for Supervision**

For RefSR online learning for SISR models in Table 3, we can compare two results by $D_s^{LR} + D_s^{Ref}$ and $D_s^{Pse} + D_s^{Ref}$. With high similarity levels (i.e., XH and H), $D_s^{LR} + D_s^{Ref}$ shows better performance while $D_s^{Pse} + D_s^{Ref}$ works better for low similarity levels (i.e., M, L, and XL). For XH and H reference images, baseline networks can exploit highly relevant information from them, as we inspected. However, the role of D_s^{Ref} is weakened with irrelevant reference images, while that of the combined data, D_s^{LR} or D_s^{Pse} , is relatively emphasized. Therefore, the performance improvement from D_s^{Ref} combined with D_s^{Pse} is superior, thanks to the knowledge from a pre-trained model (i.e., D_s^{Pse}), compared to the self-supervision (i.e., D_s^{LR}). Meanwhile, for RefSR online learning for RefSR models, fine-tuning with \bar{I}^{HR} achieves better overall performance than fine-tuning with I^{LR} . In other words, for all similarity levels, $D_r^{Pse} + D_r^{Ref2}$ shows better performance than $D_r^{LR} + D_r^{Ref1}$, as reported in Table 4. The reason for this is that \bar{I}^{HR} has a relatively similar resolution to I^{Ref} than I^{LR} ; thus, it is much easier to align and combine with the information in the reference image.

- **Non-Bicubic Degradation**

We further validate our algorithm with a LR image with non-bicubic degradation for both RCAN (SISR) and TTSR (RefSR) models. For non-bicubic $\times 4$ degradation, we have utilized isotropic (g_w) and anisotropic (g_{ani}) Gaussian kernels of width w with direct (g^d) and bicubic (g^b) subsampling methods presented in MZSR [36]. Table 5 shows that RCAN and TTSR pre-trained with bicubic degradation produce inferior SR results because they cannot handle non-bicubic degradation. However, RCAN and TTSR models can achieve substantial performance gains with the proposed online learning if the non-bicubic degradation model is given during the online learning (i.e., Non-blind). Moreover, RCAN and TTSR can be improved during the online learning in a blind manner that is conducted using each input obtained by downsampling with a random kernel [36]. Figure 2 shows qualitative non-bicubic comparisons between existing methods and ours. Therefore, we conclude that the proposed method can handle any type of degradation (i.e., bicubic and non-bicubic), regardless of the awareness of the degradation kernel (i.e., blind and non-blind).

Table 5. Online learning results with non-bicubic degradation.

Model	Kernel	Blind	Method	PSNR	SSIM	LPIPS	Model	Kernel	Blind	Method	PSNR	SSIM	LPIPS											
Ours+ EDSR [5]	$\delta_{0.2}^d$	-	Pre-trained	18.754	0.534	0.4068	Ours+ SSEN [20]	$\delta_{0.2}^d$	-	Pre-trained	18.538	0.521	0.4142											
		Non-blind	$D_s^{LR} + D_s^{Ref}$	24.335	0.726	0.3035			Non-blind	D_r^{Ref1} D_r^{Ref2}	23.565	0.694	0.3431	24.155	0.720	0.3239								
	$\delta_{2.0}^d$	-	Pre-trained	21.387	0.606	0.3771		$\delta_{2.0}^d$	-	Pre-trained	20.706	0.586	0.3541	$\delta_{2.0}^d$	Non-blind	D_r^{Ref1} D_r^{Ref2}	25.436	0.741	0.2891	26.105	0.765	0.2838		
		Non-blind	$D_s^{LR} + D_s^{Ref}$	26.263	0.772	0.2665			Non-blind	D_r^{Ref1} D_r^{Ref2}	25.436	0.741	0.2891		26.105	0.765	0.2838							
	$\delta_{1.3}^b$	-	Pre-trained	21.364	0.593	0.3639		$\delta_{1.3}^b$	-	Pre-trained	21.269	0.590	0.3633	$\delta_{1.3}^b$	Non-blind	D_r^{Ref1} D_r^{Ref2}	25.213	0.728	0.3062	25.882	0.753	0.2953		
		Non-blind	$D_s^{LR} + D_s^{Ref}$	26.164	0.765	0.2764			Non-blind	D_r^{Ref1} D_r^{Ref2}	25.213	0.728	0.3062		25.882	0.753	0.2953							
	-	-	Pre-trained	25.595	0.741	0.3288		-	-	Pre-trained	25.522	0.740	0.3273	-	Non-blind	D_r^{Ref1} D_r^{Ref2}	26.010	0.758	0.2773	26.569	0.778	0.2789		
		Blind	$D_s^{LR} + D_s^{Ref}$	24.354	0.697	0.3459			Blind	D_r^{Ref1} D_r^{Ref2}	23.953	0.676	0.3654		24.201	0.685	0.3608							
	Ours+ RCAN [7]	$\delta_{0.2}^d$	-	Pre-trained	17.938	0.497		0.4111	Ours+ TTSR- rec [21]	$\delta_{0.2}^d$	-	Pre-trained	18.415	0.524	0.4039	$\delta_{0.2}^d$	Non-blind	D_r^{Ref1} D_r^{Ref2}	23.489	0.688	0.3423	24.168	0.717	0.3232
			Non-blind	$D_s^{LR} + D_s^{Ref}$	24.532	0.737		0.2910			Non-blind	D_r^{Ref1} D_r^{Ref2}	23.489	0.688	0.3423		24.168	0.717	0.3232					
		$\delta_{2.0}^d$	-	Pre-trained	21.131	0.597		0.3335		$\delta_{2.0}^d$	-	Pre-trained	21.211	0.609	0.3127	$\delta_{2.0}^d$	Non-blind	D_r^{Ref1} D_r^{Ref2}	25.911	0.760	0.2647	26.561	0.784	0.2624
			Non-blind	$D_s^{LR} + D_s^{Ref}$	26.545	0.783		0.2586			Non-blind	D_r^{Ref1} D_r^{Ref2}	25.911	0.760	0.2647		26.561	0.784	0.2624					
$\delta_{1.3}^b$		-	Pre-trained	21.198	0.587	0.3609	$\delta_{1.3}^b$	-		Pre-trained	21.199	0.596	0.3367	$\delta_{1.3}^b$	Non-blind	D_r^{Ref1} D_r^{Ref2}	25.512	0.741	0.2841	26.199	0.768	0.2754		
		Non-blind	$D_s^{LR} + D_s^{Ref}$	26.414	0.775	0.2679		Non-blind		D_r^{Ref1} D_r^{Ref2}	25.512	0.741	0.2841		26.199	0.768	0.2754							
-		-	Pre-trained	25.484	0.738	0.3314	-	-		Pre-trained	26.147	0.767	0.2912	-	Non-blind	D_r^{Ref1} D_r^{Ref2}	26.599	0.781	0.2471	26.989	0.796	0.2471		
		Blind	$D_s^{LR} + D_s^{Ref}$	24.277	0.692	0.3480		Blind		D_r^{Ref1} D_r^{Ref2}	23.928	0.672	0.3535		24.010	0.684	0.3461							

5. Conclusions

We have proposed an online learning algorithm for RefSR to exploit various types of data for network adaptation in the test stage. The proposed method has brought significant performance improvements to both SISR and RefSR models without introducing any additional network parameters. Specifically, various types of data pairs are proposed using input LR, pseudo-HR, and reference HR images, and the role of each data pair is verified with different similarity levels of the reference images. Extensive experimental results demonstrate the validity, efficiency, and versatility of the proposed algorithm.

Author Contributions: Conceptualization, D.C.; formal analysis, J.P.; investigation, T.-H.K. and D.C.; data curation, B.C.; writing—original draft preparation, D.C.; writing—review and editing, T.-H.K. and D.C.; supervision, D.C. and J.P.; funding acquisition, D.C. All authors have read and agreed to the published version of the manuscript.

Funding: This work was supported by BK21 FOUR Program by Chungnam National University Research Grant, 2021–2022.

Conflicts of Interest: The authors declare no conflict of interest.

References

1. Dong, C.; Loy, C.C.; Tang, X. Accelerating the super-resolution convolutional neural network. In Proceedings of the 14th European Conference on Computer Vision (ECCV), Amsterdam, The Netherlands, 8–16 October 2016; pp. 391–407.
2. Shi, W.; Caballero, J.; Huszár, F.; Totz, J.; Aitken, A.P.; Bishop, R.; Rueckert, D.; Wang, Z. Real-Time Single Image and Video Super-Resolution Using an Efficient Sub-Pixel Convolutional Neural Network. In Proceedings of the 2016 IEEE Conference on Computer Vision and Pattern Recognition (CVPR), Las Vegas, NV, USA, 27–30 June 2016; pp. 1874–1883.
3. Kim, J.; Lee, J.K.; Lee, K.M. Accurate Image Super-Resolution Using Very Deep Convolutional Networks. In Proceedings of the 2016 IEEE Conference on Computer Vision and Pattern Recognition (CVPR), Las Vegas, NV, USA, 27–30 June 2016; pp. 1646–1654.
4. Kim, J.; Lee, J.K.; Lee, K.M. Deeply-Recursive Convolutional Network for Image Super-Resolution. In Proceedings of the 2016 IEEE Conference on Computer Vision and Pattern Recognition (CVPR), Las Vegas, NV, USA, 27–30 June 2016; pp. 1637–1645.
5. Lim, B.; Son, S.; Kim, H.; Nah, S.; Lee, K.M. Enhanced Deep Residual Networks for Single Image Super-Resolution. In Proceedings of the 2017 IEEE Conference on Computer Vision and Pattern Recognition Workshops (CVPRW), Honolulu, HI, USA, 21–26 July 2017; pp. 1132–1140.
6. Dai, T.; Cai, J.; Zhang, Y.; Xia, S.T.; Zhang, L. Second-Order Attention Network for Single Image Super-Resolution. In Proceedings of the 2019 IEEE/CVF Conference on Computer Vision and Pattern Recognition (CVPR), Long Beach, CA, USA, 15–20 June 2019; pp. 11065–11074.
7. Zhang, Y.; Li, K.; Li, K.; Wang, L.; Zhong, B.; Fu, Y. Image Super-Resolution Using Very Deep Residual Channel Attention Networks. In Proceedings of the 2018 European Conference on Computer Vision (ECCV), Munich, Germany, 8–14 September 2018; pp. 286–301.
8. Zhang, Y.; Tian, Y.; Kong, Y.; Zhong, B.; Fu, Y. Residual Dense Network for Image Super-Resolution. In Proceedings of the 2018 IEEE/CVF Conference on Computer Vision and Pattern Recognition (CVPR), Salt Lake City, UT, USA, 18–23 June 2018; pp. 2472–2481.
9. Dong, C.; Loy, C.C.; He, K.; Tang, X. Image Super-Resolution Using Deep Convolutional Networks. *IEEE Trans. Pattern Anal. Mach. Intell. (TPAMI)* **2016**, *38*, 295–307. [[CrossRef](#)] [[PubMed](#)]
10. Sajjadi, M.S.M.; Scholkopf, B.; Hirsch, M. EnhanceNet: Single Image Super-Resolution through Automated Texture Synthesis. In Proceedings of the 2017 IEEE International Conference on Computer Vision (ICCV), Venice, Italy, 22–29 October 2017; pp. 4501–4510.
11. Ledig, C.; Theis, L.; Huszar, F.; Caballero, J.; Cunningham, A.; Acosta, A.; Aitken, A.; Tejani, A.; Totz, J.; Wang, Z.; et al. Photo-Realistic Single Image Super-Resolution Using a Generative Adversarial Network. In Proceedings of the 2017 IEEE Conference on Computer Vision and Pattern Recognition (CVPR), Honolulu, HI, USA, 21–26 July 2017; pp. 4681–4690.
12. Johnson, J.; Alahi, A.; Fei-Fei, L. Perceptual losses for real-time style transfer and super-resolution. In Proceedings of the 14th European Conference on Computer Vision (ECCV), Amsterdam, The Netherlands, 8–16 October 2016; pp. 694–711.
13. Liu, C.; Sun, D. A Bayesian approach to adaptive video super resolution. In Proceedings of the Computer Vision and Pattern Recognition (CVPR), Colorado Springs, CO, USA, 20–25 June 2011; pp. 209–216.
14. Caballero, J.; Ledig, C.; Aitken, A.P.; Acosta, A.; Totz, J.; Wang, Z.; Shi, W. Real-Time Video Super-Resolution with Spatio-Temporal Networks and Motion Compensation. In Proceedings of the 2017 IEEE Conference on Computer Vision and Pattern Recognition (CVPR), Honolulu, HI, USA, 21–26 July 2017; pp. 2848–2857.
15. Yue, H.; Sun, X.; Yang, J.; Wu, F. Landmark Image Super-Resolution by Retrieving Web Images. *IEEE Trans. Image Process. (TIP)* **2013**, *22*, pp. 4865–4878.
16. Lowe, D.G. Object recognition from local scale-invariant features. In Proceedings of the Seventh IEEE International Conference on Computer Vision, Kerkyra, Greece, 20–27 September 1999; pp. 1150–1157.
17. Wu, Y.; Ma, W.; Gong, M.; Su, L.; Jiao, L. A Novel Point-Matching Algorithm Based on Fast Sample Consensus for Image Registration. *IEEE Geosci. Remote Sens. Lett.* **2014**, *12*, 43–47. [[CrossRef](#)]
18. Sarlin, P.E.; DeTone, D.; Malisiewicz, T.; Rabinovich, A. SuperGlue: Learning Feature Matching With Graph Neural Networks. In Proceedings of the 2020 IEEE/CVF Conference on Computer Vision and Pattern Recognition (CVPR), Seattle, WA, USA, 13–19 June 2020; pp. 4938–4947.
19. Zheng, H.; Ji, M.; Han, L.; Xu, Z.; Wang, H.; Liu, Y.; Fang, L. Learning Cross-scale Correspondence and Patch-based Synthesis for Reference-based Super-Resolution. In Proceedings of the 28th British Machine Vision Conference (BMVC), Imperial College, London, 4–7 September 2017; pp. 138.1–138.13.
20. Shim, G.; Park, J.; Kweon, I.S. Robust Reference-Based Super-Resolution With Similarity-Aware Deformable Convolution. In Proceedings of the 2020 IEEE/CVF Conference on Computer Vision and Pattern Recognition (CVPR), Seattle, WA, USA, 13–19 June 2020; pp. 8425–8434.
21. Yang, F.; Yang, H.; Fu, J.; Lu, H.; Guo, B. Learning Texture Transformer Network for Image Super-Resolution. In Proceedings of the 2020 IEEE/CVF Conference on Computer Vision and Pattern Recognition (CVPR), Seattle, WA, USA, 13–19 June 2020; pp. 5790–5799.
22. Assaf Shocher, Nadav Cohen, M.I. “Zero-Shot” Super-Resolution using Deep Internal Learning. In Proceedings of the 2018 IEEE/CVF Conference on Computer Vision and Pattern Recognition (CVPR), Salt Lake City, UT, USA, 18–23 June 2018; pp. 3118–3126.

23. Glasner, D.; Bagon, S.; Irani, M. Super-resolution from a single image. In Proceedings of the 2009 IEEE 12th International Conference on Computer Vision, Kyoto, Japan, 29 September–2 October 2009; pp. 349–356.
24. Zontak, M.; Irani, M. Internal statistics of a single natural image. In Proceedings of the Computer Vision and Pattern Recognition (CVPR), Colorado Springs, CO, USA, 20–25 June 2011; pp. 977–984.
25. Dong, C.; Loy, C.C.; He, K.; Tang, X. Learning a Deep Convolutional Network for Image Super-Resolution. In Proceedings of the 13th European Conference on Computer Vision (ECCV), Zurich, Switzerland, 6–12 September 2014; pp. 184–199.
26. Lai, W.; Huang, J.; Ahuja, N.; Yang, M. Deep Laplacian Pyramid Networks for Fast and Accurate Super-Resolution. In Proceedings of the 2017 IEEE Conference on Computer Vision and Pattern Recognition (CVPR), Honolulu, HI, USA, 21–26 July 2017; pp. 5835–5843.
27. Wang, X.; Yu, K.; Wu, S.; Gu, J.; Liu, Y.; Dong, C.; Qiao, Y.; Loy, C.C. ESRGAN: Enhanced Super-Resolution Generative Adversarial Networks. In Proceedings of the 2018 European Conference on Computer Vision Workshops (ECCVW), Munich, Germany, 8–14 September 2018; pp. 63–79.
28. Dosovitskiy, A.; Fischer, P.; Ilg, E.; Häusser, P.; Hazirbas, C.; Golkov, V.; van der Smagt, P.; Cremers, D.; Brox, T. FlowNet: Learning Optical Flow with Convolutional Networks. In Proceedings of the 2015 IEEE International Conference on Computer Vision (ICCV), Santiago, Chile, 7–13 December 2015; pp. 2758–2766.
29. Ilg, E.; Mayer, N.; Saikia, T.; Keuper, M.; Dosovitskiy, A.; Brox, T. FlowNet 2.0: Evolution of Optical Flow Estimation with Deep Networks. In Proceedings of the 2017 IEEE Conference on Computer Vision and Pattern Recognition (CVPR), Honolulu, HI, USA, 21–26 July 2017; pp. 1647–1655.
30. Zheng, H.; Ji, M.; Wang, H.; Liu, Y.; Fang, L. CrossNet: An End-to-end Reference-based Super Resolution Network using Cross-scale Warping. In Proceedings of the 2018 European Conference on Computer Vision (ECCV), Munich, Germany, 8–14 September 2018; pp. 88–104.
31. Gatys, L.; Ecker, A.S.; Bethge, M. Texture Synthesis Using Convolutional Neural Networks. In Proceedings of the Twenty-ninth Conference on Neural Information Processing Systems (NeurIPS), Montreal, Quebec, Canada, 7–12 December 2015; pp. 262–270.
32. Gatys, L.A.; Ecker, A.S.; Bethge, M. Image Style Transfer Using Convolutional Neural Networks. In Proceedings of the 2016 IEEE Conference on Computer Vision and Pattern Recognition (CVPR), Las Vegas, NV, USA, 27–30 June 2016; pp. 2414–2423.
33. Zhang, Z.; Wang, Z.; Lin, Z.; Qi, H. Image Super-Resolution by Neural Texture Transfer. In Proceedings of the 2019 IEEE/CVF Conference on Computer Vision and Pattern Recognition (CVPR), Long Beach, CA, USA, 15–20 June 2019; pp. 7974–7983.
34. Jiang, Y.; Chan, K.C.; Wang, X.; Loy, C.C.; Liu, Z. Robust Reference-based Super-Resolution via C2-Matching. In Proceedings of the 2021 IEEE/CVF Conference on Computer Vision and Pattern Recognition (CVPR), Nashville, TN, USA, 20–25 June 2021; pp. 2103–2112.
35. Lu, L.; Li, W.; Tao, X.; Lu, J.; Jia, J. MASA-SR: Matching Acceleration and Spatial Adaptation for Reference-Based Image Super-Resolution. In Proceedings of the 2021 IEEE/CVF Conference on Computer Vision and Pattern Recognition (CVPR), Nashville, TN, USA, 20–25 June 2021; pp. 6368–6377.
36. Soh, J.W.; Cho, S.; Cho, N.I. Meta-Transfer Learning for Zero-Shot Super-Resolution. In Proceedings of the 2020 IEEE/CVF Conference on Computer Vision and Pattern Recognition (CVPR), Seattle, WA, USA, 13–19 June 2020; pp. 3516–3525.
37. Park, S.; Yoo, J.; Cho, D.; Jiwon Kim.; Kim, T.H. Fast Adaptation to Super-Resolution Networks via Meta-learning. In Proceedings of the 16th European Conference on Computer Vision (ECCV), Glasgow, United Kingdom, 23–28 August 2020; pp. 754–769.
38. Yoo, J.; Kim, T.H. Self-Supervised Adaptation for Video Super-Resolution. *arXiv* **2021**, arXiv:2103.10081.